SUPPLEMENTARY METHODS

Electronic energy calculations

In order to achieve the highest possible accuracy in our electronic energy calculations, we carried out a three stage optimization process, using increasing accuracy at each stage. This allowed us to explore a much larger region of polymorph space than would have been possible with RPA calculations alone. Our procedure is described as follows:

Stage 1: Firstly, we optimised 15 structures, including all structures reported in Table I of the Supplementary Information of Li *et al* [37], supplemented by various hexagonal polymorphs. Some additional structures, including the highly competitive Cm–2 structure, were found by good fortune – we accidentally mis-entered coordinates for some structures that led to new stable polymorphs after optimisation. All initial structures were optimised at the LDA [9], PBE [10], D3 [13,14], D3(BJ) [15], MBD [16], and FI [17] levels and then ranked according to energy. We then identified eight structures that were energetically competitive (within 10 kJ/mol) with respect to the lowest energy structure in *all* dispersion corrected theories, which gave us confidence that the lowest energy structure would be part of this selection. The relative electronic energies of some of these selected low energy structures are reported in Supplementary Table 2, where they are compared against RPA results calculated in Stages 2 and 3 below.

Stage 2: We next carried out RPA calculations on the eight lowest energy structures using an energy cutoff of 480 eV. We used $\vec{k}$-grids of $12 \times 12 \times 12$ (for c–BN, modified appropriately for structures with multiple formula units) for the exact exchange (EXX) calculations, and $7 \times 7 \times 7$ for the RPA correlation energy calculations. Other than this we used recommended settings because of the well-behaved insulator nature of BN. This allowed us to identify c–BN, h–BN(AA') and m–BN as the lowest energy structures, whose energies needed to be further refined to establish clearly the final rankings.

Stage 3: Finally, we recalculated electronic energies for the three lowest energy structures using an increased energy cutoff of 550 eV and carried out two new sets of calculations using $10 \times 10 \times 10$ and $12 \times 12 \times 12$ $\vec{k}-$grids for both the EXX and RPA calculations, to increase accuracy. We then compared energy differences $E_{g1} = E_{\mathrm{h-BN}(AA')} - E_{\mathrm{c-BN}}$, $E_{g2} = E_{\mathrm{m-BN}} - E_{\mathrm{c-BN}}$ and $E_{g3} = E_{\mathrm{m-BN}} - E_{\mathrm{h-BN}(AA')}$ for EXX and RPA energies separately

between the two calculations and found they were sufficiently well converged to use in the free energy calculations. Key results in meV per formula unit (f.u.) are summarised in the Supplementary Table 1. (We use energy units of meV/f.u. to explain our convergence tests because these are most commonly employed in such a context.) We carried out additional EXX calculations with an energy cut-off of 850 eV, which gave essentially identical results to the 550 eV calculations, further validating our energy results.

These calculations also allowed us to identify the primary source of error as being the exact exchange term. The difference at the EXX level was 1.4 meV, 1.4 meV and 0.0 meV for E_{g1}, E_{g2} and E_{g3} respectively. For RPA they were 0.1 meV, 0.2 meV and 0.1 meV respectively, significantly less than the corresponding EXX terms. The coarse $7 \times 7 \times 7$ grid used for other structures gave RPA errors that were similar to those of EXX. Note, the essentially zero difference for E_{g3} is not surprising – both h–BN(AA') and m–BN have very similar structures and thus benefit from additional error cancellations. Finally, we used our results to quantify the expected error in our lowest energy calculations as 2 meV/f.u., or 0.2 kJ/mol for gaps between c–BN and the other low-energy structures, and 0.2 meV/f.u. = 0.02 kJ/mol between the more similar layered structures.

Free energy calculations

After calculating the electronic energies, we needed to consider quantum nuclear and T–driven vibrational effects in order to estimate Gibbs free energies. This requires numerous force–constant matrix calculations in supercells where the atoms are slightly displaced from their equilibrium positions [27,35]. Calculating these properties at the RPA level would have been prohibitively expensive. To overcome this limitation we thus took advantage of a convenient property of typical electronic systems – that the LDA is far more accurate for force derivatives than it is for energies or forces, which is believed to arise from the good hole-normalisation in LDA.

This property is closely related to the long-known ability of LDA to predict good elastic coefficients, which has been confirmed in various h–BN structures in recent work [36] and further confirmed here (Table 1 in the main text), via direct elastic coefficient calculations carried out at RPA and LDA levels. We thus used LDA to calculate quantum nuclear effects and T–induced vibrational excitations in bulk BN. Supplementary Figure 5 shows that the

ZPE differences calculated with LDA and PBE-D3 are very similar, further validating our choice to use LDA.

$F_{\rm vib}$ correction due to phonon uncertainties $\delta\omega$

The analytical expression of the vibrational free energy is:

$$F_{\rm vib}(V,T) = \frac{1}{N_q}\, k_B T \sum_{\boldsymbol{q}s} \ln\left[2\sinh\left(\frac{\hbar\omega_{\boldsymbol{q}s}}{2k_{\rm B}T}\right)\right] \ , \tag{1}$$

where N_q is the total number of wave vectors used for integration within the first Brillouin zone, the summation runs over all wave vectors $\boldsymbol{q}$ and phonon branches s, and $\omega_{\boldsymbol{q}s}$ are the vibrational frequencies of the crystal, which depend on volume.

The change in $F_{\rm vib}$, $\delta F_{\rm vib}$, due to small corrections on the phonons, $\delta\omega$, is:

$$\begin{aligned} \delta F_{\rm vib} &= \frac{\partial F_{\rm vib}}{\partial\omega}\cdot\delta\omega \\ &= \frac{\delta\omega}{\omega}\cdot\frac{1}{2N_q}\sum_{\boldsymbol{q}s}\frac{\hbar\omega_{\boldsymbol{q}s}}{\tanh\left(\frac{\hbar\omega_{\boldsymbol{q}s}}{2k_{\rm B}T}\right)} \ . \end{aligned} \tag{2}$$

For the regime of low temperatures in which we are interested, $\tanh\left(\frac{\hbar\omega}{2k_{\rm B}T}\right) \approx 1$ hence $\delta F_{\rm vib}$ reduces to:

$$\begin{aligned} \delta F_{\rm vib} &= \frac{\delta\omega}{\omega}\cdot\frac{1}{2N_q}\sum_{\boldsymbol{q}s}\hbar\omega_{\boldsymbol{q}s} \\ &= \frac{\delta\omega}{\omega}\cdot E_{ZPE} \ , \end{aligned} \tag{3}$$

where E_{ZPE} is the zero-point energy.

Corrections on the phonon frequencies are likely to be the same as on the elastic constants, since both quantities are estimated through second derivatives of the energy; consequently, Eq.(3) can be approximated by:

$$|\delta F_{\rm vib}| \approx \left|\frac{\delta B_{VRH}}{B_{VRH}}\right| \cdot |E_{ZPE}| \ , \tag{4}$$

where B_{VRH} is the bulk modulus in the Voigt-Reuss-Hill approximation as estimated directly from the elastic constants and $\delta B_{VRH} \equiv B_{VRH}^{RPA} - B_{VRH}^{LDA}$.

Finally, let us turn to the cases considered here. We find $|\frac{\delta B_{VRH}}{B_{VRH}}| = 0.06$ for the difference between RPA and LDA values in both c-BN and h-BN(AA'). The difference of ZPE

between these polymorphs is E_{ZPE}(c-BN) − E_{ZPE}(h-BN(AA')) = 1 kJ/mol, which leads to $|\delta\Delta G_{\mathrm{c-h}}|$ = 0.06 kJ/mol. We use this value as the additional source of error in our calculations coming from the use of LDA phonons.

	$10 \times 10 \times 10$			$12 \times 12 \times 12$		
Energy difference	EXX	RPA	Tot.	EXX	RPA	Tot.
$E_{\mathrm{h-BN}(AA')} - E_{\mathrm{c-BN}}$	-421.1	448.2	27.1	-422.5	448.1	25.6
$E_{\mathrm{m-BN}} - E_{\mathrm{c-BN}}$	-406.9	434.5	27.5	-408.3	434.3	26.0
$E_{\mathrm{m-BN}} - E_{\mathrm{h-BN}(AA')}$	14.2	-13.8	0.4	14.2	-13.8	0.4

Supplementary Table I: Numerical tests performed for **Stage 3** in the RPA calculations.

Polymorph	LDA [9]	PBE [10]	MBD [16]	FI [17]	D3(BJ) [15]	D3 [13,14]	**RPA** [22-26]
h-BN(AA')	11.5	*-13.9*	3.4	1.2	0.5	*-4.2*	**2.5**
m-BN	11.5	*-12.4*	3.2	2.0	0.5	*-3.2*	**2.5**
h-BN(AB)	11.3	*-13.6*	3.2	1.3	0.4	*-4.0*	**2.6**
h-BN(ABC)	11.8	*-13.3*	3.2	1.6	0.9	*-3.6*	**2.8**
h-BN(ABA)	12.2	*-13.8*	4.0	1.9	1.1	*-3.5*	**3.6**
w-BN	3.5	3.7	3.7	3.8	3.6	3.9	**3.7**
h-BN(AA)	13.9	*-13.6*	5.7	3.6	2.5	*-2.1*	**5.0**

Supplementary Table II: Zero-temperature electronic energies (i.e., neglecting zero-point energy corrections) of several BN polymorphs as compared to that of the c–BN (space group $F\bar{4}3m$) phase. Italics indicate energies below that of the c–BN phase, and indicate a major failure of the given method to predict the correct ordering. Inclusion of dispersion corrections is vital, but most dispersion methods give, at best, semi-quantitative agreement with RPA (bold). This highlights the need for high-level theory when studying different polymorphs. Results are in units of kJ/mol. The same data expressed in meV per formula unit appear just below.

Polymorph	LDA [9]	PBE [10]	MBD [16]	FI [17]	D3(BJ) [15]	D3 [13,14]	**RPA** [22-26]
h–BN(AA')	118.8	*-144.0*	35.0	5.5	12.2	*-43.4*	**25.6**
m–BN	118.8	*-128.6*	33.4	5.7	20.6	*-33.5*	**26.0**
h–BN(AB)	117.4	*-141.2*	33.0	4.1	13.4	*-41.0*	**27.2**
h–BN(ABC)	121.8	*-138.1*	33.2	9.4	16.4	*-37.8*	**29.5**
h–BN(ABA)	126.3	*-142.7*	41.9	19.8	11.7	*-36.2*	**37.7**
w–BN	36.1	38.7	38.1	37.5	39.5	40.6	**38.8**
h–BN(AA)	144.1	*-141.2*	59.5	36.9	25.9	*-22.2*	**51.6**

Method	a (Å)	b (Å)	c (Å)	α (°)	β (°)	γ (°)	B Wyckoff position	N Wyckoff position
LDA [7]	4.31	2.49	3.55	90	115	90	(0.667,0.500,0.001)	(0.000,0.500,0.999)
PBE [8]	4.35	2.51	3.96	90	113	90	(0.666,0.500,0.000)	(0.000,0.500,0.999)
PBE-D3 [11,12]	4.35	2.51	3.69	90	115	90	(0.667,0.500,0.000)	(0.000,0.500,0.000)
PBE-D3(BJ) [13]	4.34	2.51	3.60	90	115	90	(0.667,0.500,0.001)	(0.000,0.500,0.000)
MBD [14]	4.34	2.51	3.56	90	113	90	(0.666,0.500,0.000)	(0.000,0.500,0.000)
FI [15]	4.34	2.51	3.56	90	113	90	(0.666,0.500,0.000)	(0.000,0.500,0.000)

Supplementary Table III: Structural properties of the new monoclinic phase m–BN (space group Cm) reported in this study as calculated with different methods based on density functional theory. The structural data have been generated with the FINDSYM software [38] by imposing a typical lattice and position tolerance of 0.1 and 0.01 Å, respectively.

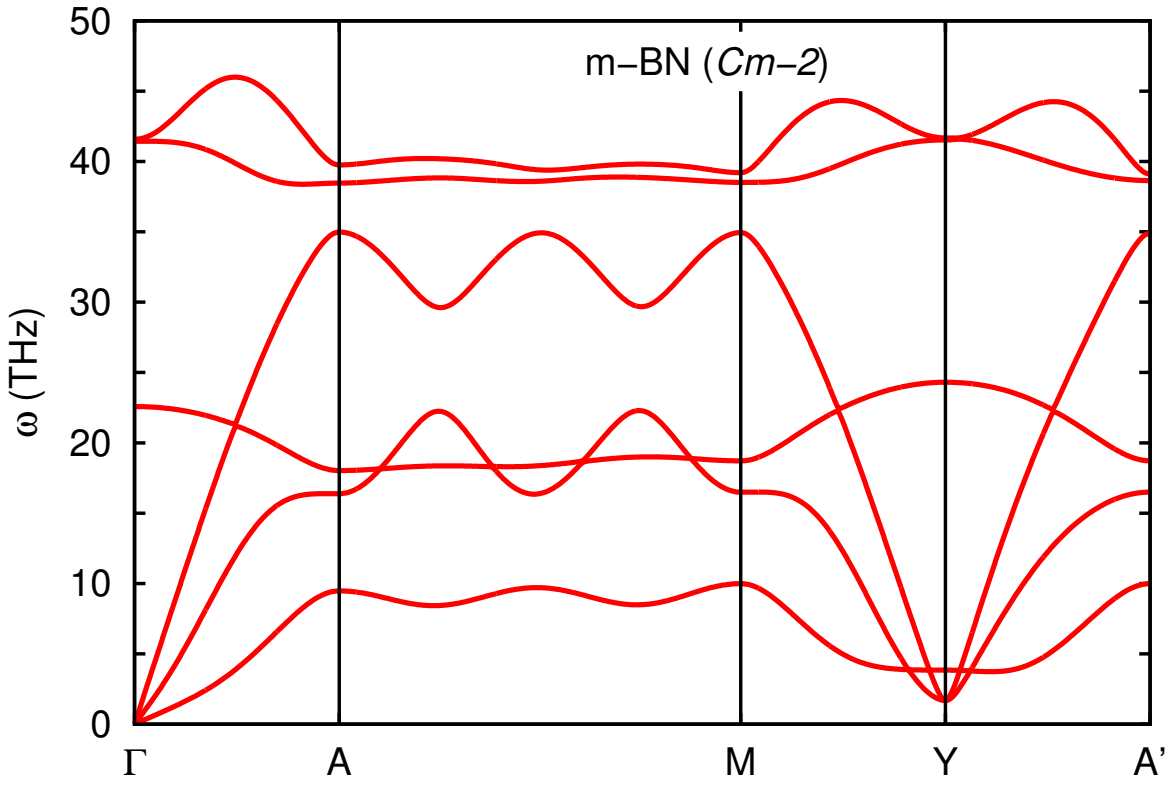

Supplementary Figure 1: Phonon spectrum of the new monoclinic phase m–BN (space group Cm) reported in this study as calculated with the LDA method at zero pressure. The system is shown to be vibrationally stable.

Polymorph	C_{11}	C_{22}	C_{33}	C_{13}	C_{23}	C_{12}	B_{VRH}	G_{VRH}	μ_{VRH}	Y_{VRH}
c–BN	997	997	997	101	101	101	402	410	0.12	920
h–BN(AA')	923	926	29	174	3	3	138	97	0.22	238
m–BN	751	839	45	156	100	68	160	132	0.17	311
h–BN(AB)	926	926	31	224	11	11	145	99	0.22	241
h–BN(ABC)	936	936	34	224	15	15	147	100	0.22	244
w–BN	989	989	1097	150	66	66	406	405	0.13	911

Supplementary Table IV: Elastic constants associated with compressive deformations, C_{ij}'s, bulk modulus, B_{VRH}, shear modulus, G_{VRH}, isotropic Poisson's ratio, μ_{VRH}, and Young's modulus, Y_{VRH}, calculated in the Voigt-Reuss-Hill approximation ("VRH", as this is appropriate for polycrystalline samples, see work [30] for the corresponding analytical expressions) with the LDA method. Results are in units of GPa.

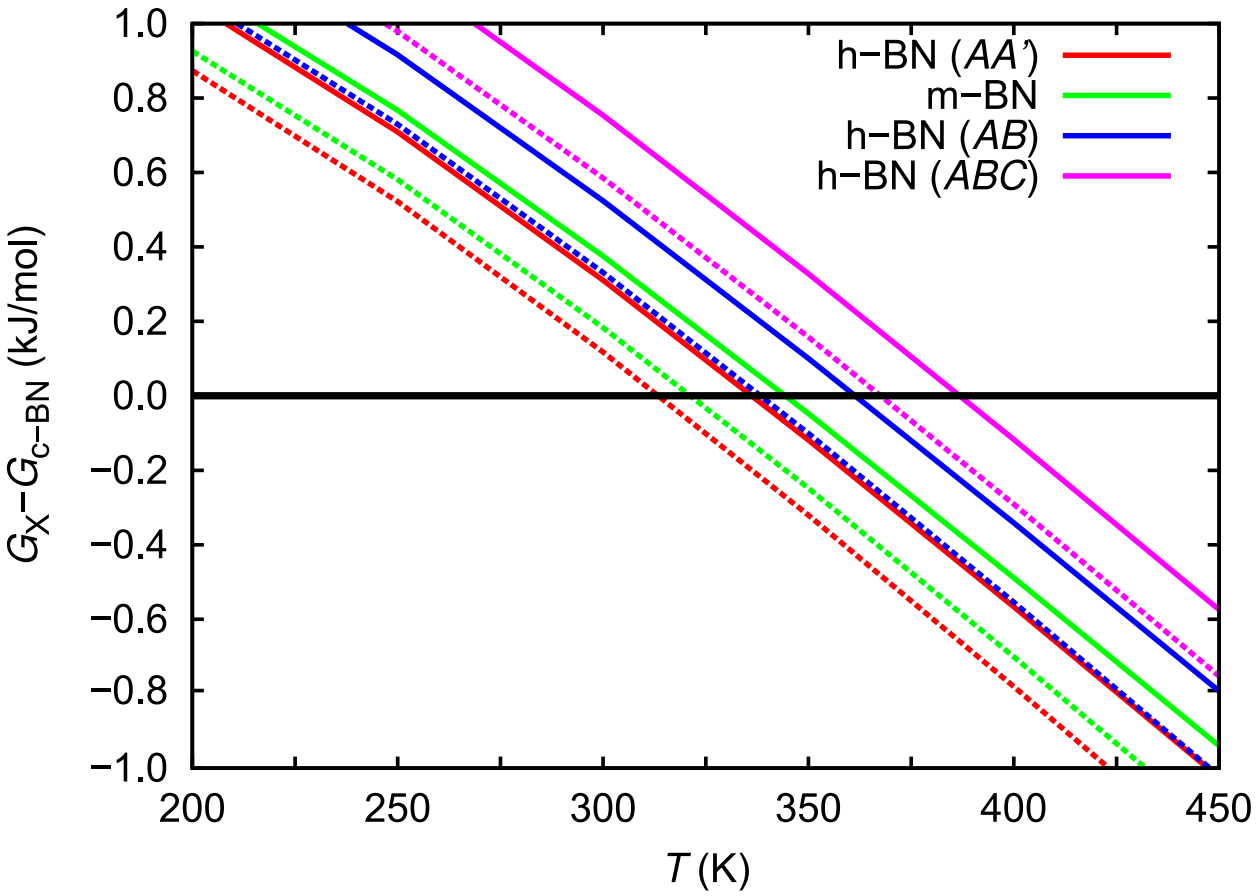

Supplementary Figure 2: Gibbs free energy differences among several BN polymorphs calculated at zero-pressure and expressed as a function of temperature. Solid lines represent results obtained by considering temperature-induced volume expansion effects, whereas dashed lines represent results obtained by neglecting such effects. When temperature-induced volume expansion effects are disregarded (dashed lines), the transition temperature for the c–BN↔h–BN(AA') transformation is underestimated by approximately 25 K.

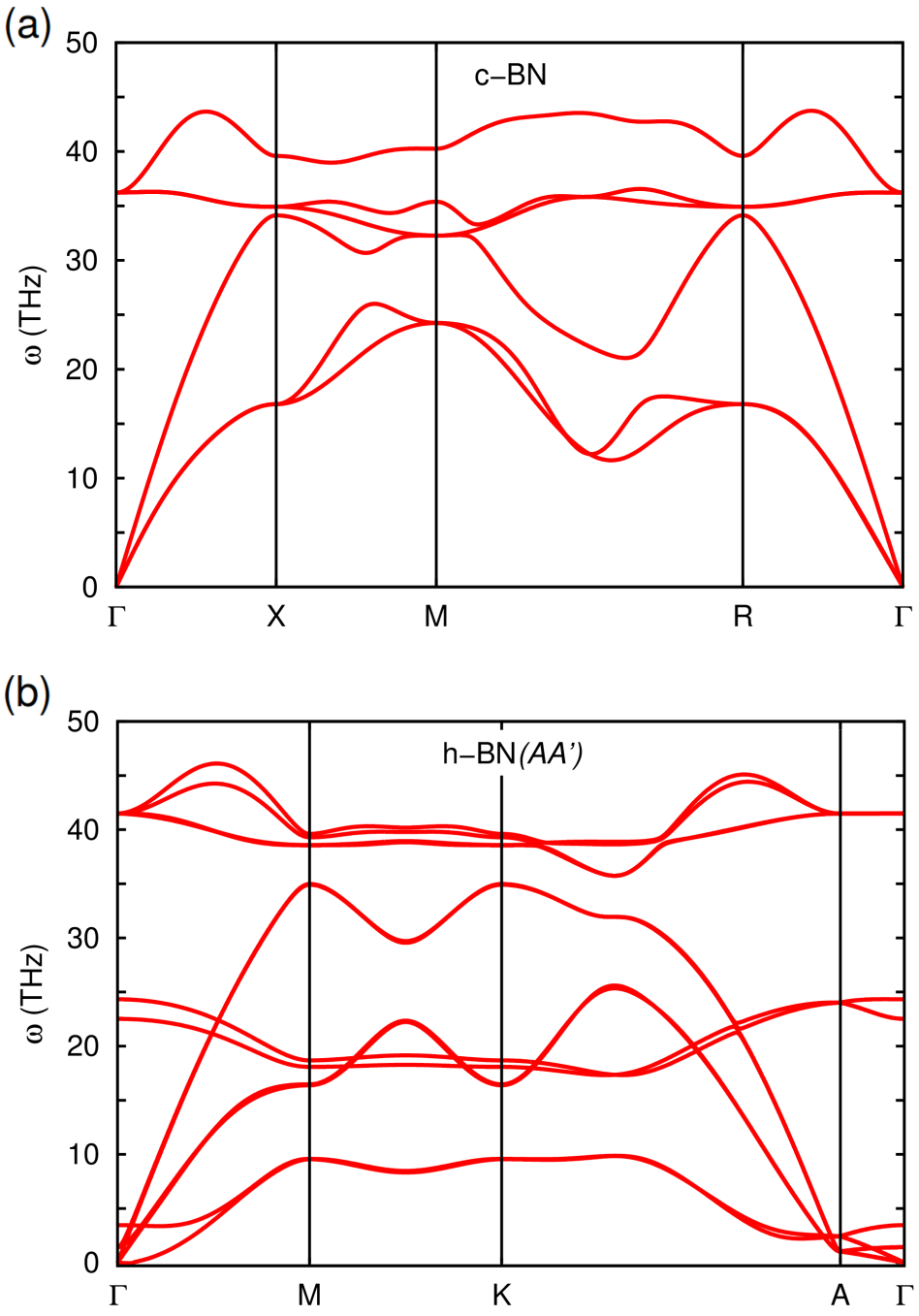

Supplementary Figure 3: Phonon spectrum of the c–BN (space group $F\bar{4}3m$) and h–BN(AA') (space group$P6_3/mmc$) polymorphs at zero pressure as calculated with the LDA method. The density of lattice excitations in the low-frequency region (that is, $\omega \leq 12$ THz) is appreciably higher in h–BN(AA') than in c–BN, hence vibrational entropy contributions to the Gibbs free energy turn out to be energetically more favourable in the hexagonal phase.

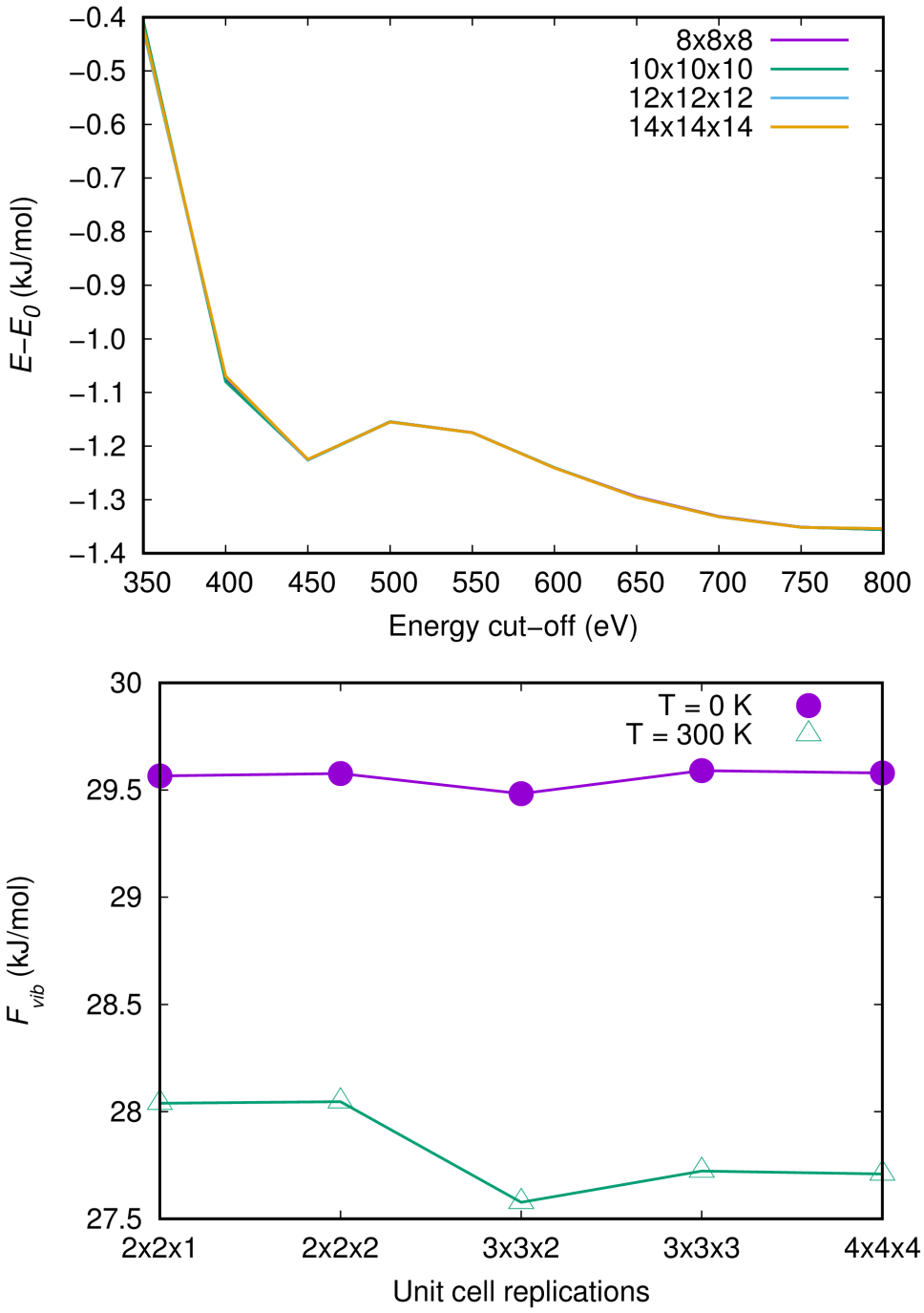

Supplementary Figure 4: Convergence tests of the electronic and vibrational free energies calculated with standard DFT methods (i.e., PBE-D3) in the h–BN(AA') polymorph. Electronic energies are converged to within 0.1 kJ/mol (1 meV per formula unit) by using an energy cut-off of 650 eV and $14 \times 14 \times 14$ **k**-point grids. Vibrational free energies are converged to within 0.1 kJ/mol (1 meV per formula unit) by considering $4 \times 4 \times 4$ simulation supercells.

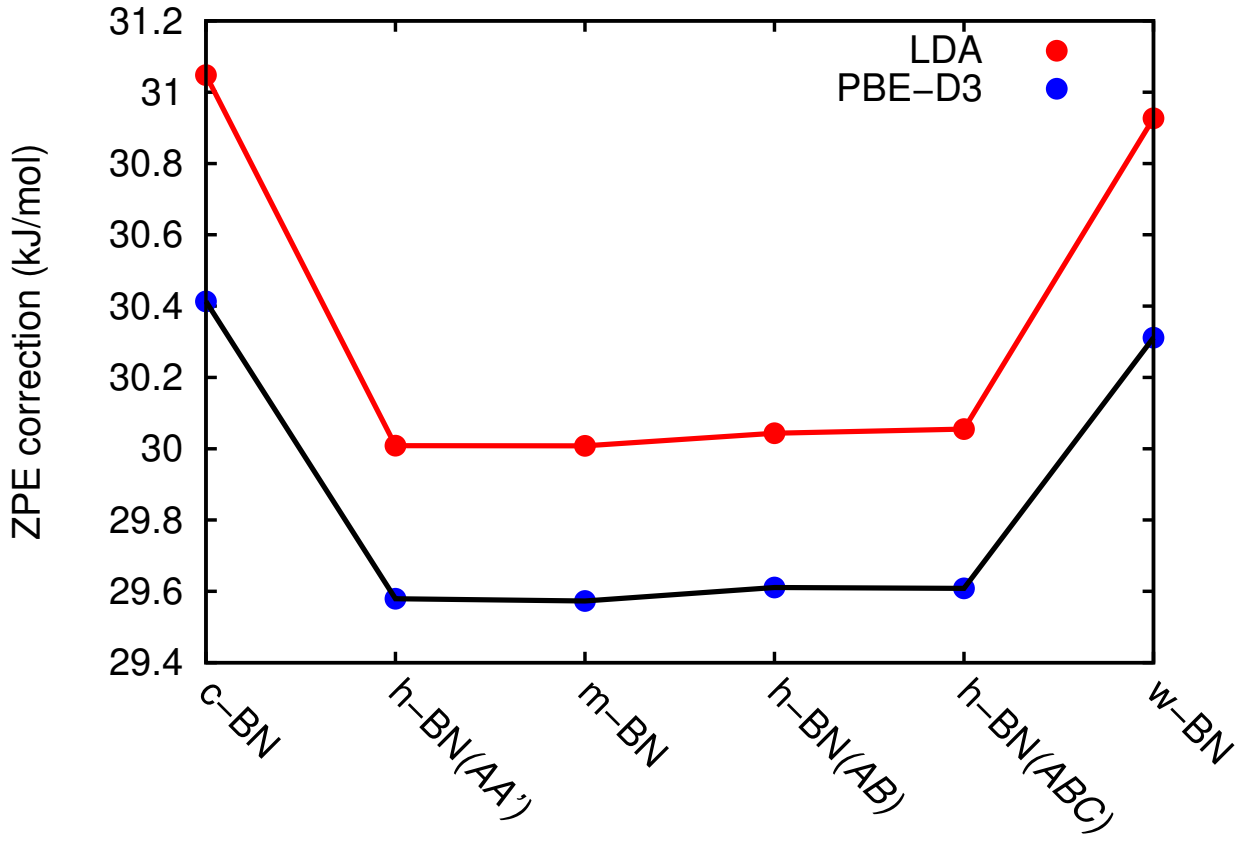

Supplementary Figure 5: Zero-point energy (ZPE) corrections accounting for zero-temperature quantum nuclear effects [27] in several BN polymorphs as calculated with the LDA [9] and PBE-D3 [13,14] methods at zero pressure. The ZPE differences estimated among BN polymorphs are practically independent of the employed method.